PCCP

Gas-Phase Synthesis of Racemic Helicenes and their Potential Role in the Enantiomeric Enrichment of Sugars and Amino Acids in Meteorites

Journal:	*Physical Chemistry Chemical Physics*
Manuscript ID	CP-ART-07-2022-003084.R1
Article Type:	Paper
Date Submitted by the Author:	16-Aug-2022
Complete List of Authors:	Kaiser, Ralf; University of Hawaii, Zhao, Long; University of Hawaii Lu, Wenchao; Lawrence Berkeley National Laboratory, Chemical Sciences Division Ahmed, Musahid; Lawrence Berkeley National Laboratory, Chemical Sciences Division Evseev, Mikhail; Samara National Research University Azyazov, Valeriy; Samara National Research University; Lebedev Physical Institute of RAS, Department of Chemical & Electric Discharge Lasers Mebel, Alexander; Florida International University, Chemistry and Biochemistry Mohamed, Rana; University of California Berkeley, Chemistry Fischer, Felix; University of California Berkeley, Chemsitry Li, Xiaohu; Xinjiang Astronomical Observatory Chinese Academy of Sciences

Gas-Phase Synthesis of Racemic Helicenes and their Potential Role in the Enantiomeric Enrichment of Sugars and Amino Acids in Meteorites

Ralf I. Kaiser,[1]* Long Zhao,[1] Wenchao Lu,[2] Musahid Ahmed,[2]* Mikhail M. Evseev,[3] Valeriy N. Azyazov,[3] Alexander M. Mebel,[4]* Rana K. Mohamed,[5] Felix R. Fischer,[5] Xiaohu Li[6]*

[1]Department of Chemistry, University of Hawaii at Manoa, Honolulu, Hawaii, 96822, USA.
Email: ralfk@hawaii.edu

[2]Chemical Sciences Division, Lawrence Berkeley National Laboratory, Berkeley, California 94720, USA. Email: mahmed@lbl.gov

[3]Lebedev Physical Institute, Samara 443011, Russia.

[4]Department of Chemistry and Biochemistry, Florida International University, Miami, Florida 33199, USA. mebela@fiu.edu

[5]Department of Chemistry, University of California, Berkeley, CA 94720, USA. Materials Sciences Division, Lawrence Berkeley National Laboratory, Berkeley, CA 94720, USA. Kavli Energy Nano Sciences Institute at the University of California Berkeley and the Lawrence Berkeley National Laboratory, Berkeley, California 94720, USA.

[6]Xinjiang Astronomical Observatory, Chinese Academy of Sciences, Urumqi, Xinjiang 830011, P.R. China. Key Laboratory of Radio Astronomy, Chinese Academy of Sciences, Urumqi, Xinjiang 830011, PR China. Email: xiaohu.li@xao.ac.cn

†Electronic supplementary information (ESI) available. See DOI:

Abstract

The molecular origins of homochirality on Earth is not understood well, particularly how enantiomerically enriched molecules of astrobiological significance like sugars and amino acids might have been synthesized on icy grains in space preceding their delivery to Earth. Polycyclic aromatic hydrocarbons (PAHs) identified in carbonaceous chondrites could have been processed in molecular clouds by circularly polarized light prior to the depletion of enantiomerically enriched helicenes onto carbonaceous grains resulting in chiral islands. However, the fundamental low temperature reaction mechanisms leading to racemic helicenes are still unknown. Here, by exploiting synchrotron based molecular beam photoionization mass spectrometry combined with electronic structure calculations, we provide compelling testimony on barrierless, low temperature pathways leading to racemates of [5] and [6]helicene. Astrochemical modeling advocates that gas-phase reactions in molecular clouds lead to racemates of helicenes suggesting a pathway for future astronomical observation and providing a fundamental understanding for the origin of homochirality on early Earth.

Introduction

The origin of biological homochirality – nature's selection of one specific enantiomer over the other – has remained a highly controversial topic[1-5] since its discovery by Louis Pasteur in 1848. Chiral molecules exist in two mirror images which are not superimposable. On Earth, living organisms developed a strict homochirality with D-sugars and L-amino acids incorporated in ribonucleic acids and polypeptides, respectively.[6] Prevalent routes to homochirality implicate the propagation and amplification of primordial enantiomeric excesses such as the identification of D-enriched sugar alcohols and sugar acids like arabinonic acid[7] along with L-enriched amino acids isovaline, α-methyl norvaline, α-methyl valine, and α-methyl norleucine in the Murchison and Murray meteorites.[8-10] These

pathways might be initiated from racemic mixtures of chiral organic molecules like amino acids,[11-15] sugars,[16] and epoxides[17] synthesized in the interstellar medium on ice-coated nanoparticles (interstellar grains) within molecular clouds, of which one enantiomer is preferentially destroyed through asymmetric beta-decay-related radiolysis[18,19] or photolytically by ultraviolet circularly polarized light in star formation regions.[20-23] Magnetars – white dwarfs with magnetic fields exceeding 10^{13} Tesla - may separate racemic mixtures of organic radicals;[24] these paramagnetic radicals may end up in spatially separated sections of the molecular clouds.[24,25] If a primordial enantiomeric excess existed in the molecular cloud, this excess could be passed on via star forming regions to its descendants (planets, moons, comets, meteorites) leading to the homochirality of life on Earth as we know it. Compelling evidence for the delivery of enantiomerically enriched organics from meteorites such as Murchison and Murray to Earth exists,[8,9] however, the question, how did D-sugars and L-amino acids outnumber L-sugars and D-amino acids is still unanswered. A fundamental understanding of the underlying pathways at the molecular, microscopic level is required to answer this question.

Here, molecular beam experiments with isomer-selective photoionization via a targeted, vinylacetylene-mediated gas-phase reaction of aromatic helicenyl radicals coupled with electronic structure calculations and astrochemical modeling reveal an elegant synthetic route to racemic helicenes - ortho-fused polycyclic aromatic hydrocarbons (PAHs),[26] in which benzene building blocks form helically-shaped molecules.[27] The simplest helicenes serve as benchmarks to unravel the exotic gas-phase chemistries leading to a facile low temperature formation of the 22- and 26-π-electron aromatic molecules [5]helicene ($C_{22}H_{14}$) and [6]helicene ($C_{26}H_{16}$) plus atomic hydrogen (1 amu) (reactions (1) and (2)), respectively. Combined with electronic structure calculations and astrochemical modeling, a molecular picture to barrierless, low temperature molecular mass growth processes of helicenes in cold molecular clouds such as TMC-1 and OMC-1 emerges through a stepwise

ring annulation one ring at a time via bimolecular gas-phase reactions of an aromatic helicenyl radical with vinylacetylene. These processes were previously conjectured to operate only at elevated temperatures of a few 1,000 K prevailing in circumstellar envelopes of carbon rich stars and planetary nebulae as their descendants since entrance barriers equivalent to a few 100 K prohibit these reactions in cold molecular clouds.[28] Accounting for the handedness of the helix, clockwise and counterclockwise helices are non-superimposable causing an axial chirality (helical chirality) with left- and right-handed helices defined by *minus* (**M**) and *plus* (**P**) (Figure 1).[29] Although the gas-phase mechanism unraveled here leads to *racemates* of [5] and [6]helicenes, i.e. mixtures of equal quantities of the **M** and **P** enantiomers, circularly polarized ultraviolet light[30] as detected toward the Orion Massive Star Forming Region[31] may preferentially photolyze the **M** or **P** enantiomer in the gas-phase of the interstellar medium. This process may initiate the complex chain of reactions ultimately leading to an enantiomeric excess in biorelevant molecules such as D-sugars and L-amino acids and possibly homochirality in our Solar System (Figure 1).

(1) $C_{18}H_{11}^{\bullet}$ (227 amu) + C_4H_4 (52 amu) → $C_{22}H_{14}$ (278 amu) + $H^{\bullet}$ (1 amu)

(2) $C_{22}H_{13}^{\bullet}$ (277 amu) + C_4H_4 (52 amu) → $C_{26}H_{16}$ (278 amu) + $H^{\bullet}$ (1 amu)

Experimental

The experiments were carried out at the Chemical Dynamics Beamline (9.0.2) of the Advanced Light Source (ALS) with a resistively-heated silicon carbide (SiC) chemical reactor interfaced to a molecular beam apparatus operated with a Wiley-McLaren reflectron time-of-flight mass spectrometer (Re-TOF-MS).[32] 2-bromobenzo[c]phenanthrene and 9-bromodibenzo[c,g] phenanthrene were synthesized following literature procedures. The [4]helicenyl radicals were prepared *in situ* via pyrolysis of the corresponding brominated precursors. Note that the low vapor pressure of the heated [5]helicenyl precursor prohibited the collection of data at an adequate signal-to-noise ration. Therefore, only a computational study was conducted for this system. The reactants were seeded at a level of less than 0.01 % in a vinylacetylene (5 %) – helium (95

%) carrier gas at 150 Torr and introduced into a resistively heated silicon carbide tube (SiC) with the temperature of 1,585 ± 85 K monitored using a Type-C thermocouple. The products formed in the reactor were expanded supersonically and passed through a 2 mm diameter skimmer located 10 mm downstream of the pyrolytic reactor and enter into the main chamber, which houses the Re-TOF-MS. Under the current experimental conditions, vinylacetylene does not pyrolyze.[33] The quasi-continuous tunable vacuum ultraviolet (VUV) light from the Advanced Light Source intercepted the neutral supersonic molecular beam perpendicularly in the extraction region of Re-TOF-MS. VUV single photon ionization is essentially a fragment-free ionization technique and hence is characterized as a *soft ionization* method.[34] The ions formed via photoionization are extracted and detected by a multichannel plate detector. Photoionization efficiency (PIE) curves, which report ion counts as a function of photon energy ranged from 7.00 to 9.50 eV, with a step interval of 0.05 eV at a well-defined mass-to-charge ratio (*m/z*), were produced by integrating the signal recorded at the specific *m/z* for the species of interest.

Theoretical Calculations. The geometric structures, vibrational frequencies, and energies of the local minima and transition states involved in the reactions of [4] and [5]helicenyl radicals with vinylacetylene were computed at the G3(MP2,CC)//B3LYP/6-311G(d,p) level of theory.[35-37] This dual-level computational approach involves geometry optimization and vibrational frequencies calculations at the density functional B3LYP level of theory with the 6-311G(d,p) basis set. Then, single-point energies of the optimized structures were refined within the framework of the G3(MP2,CC) model chemistry where the total energy of each species is computed as

$$E_0[G3(MP2,CC)] = E[CCSD(T)/6\text{-}31G(d)] + \Delta E_{MP2} + E(ZPE),$$

where ΔE_{MP2} is a basis set correction, $\Delta E_{MP2} = E[MP2/G3Large] - E[MP2/6\text{-}31G(d)]$, and E(ZPE) is the zero-point energy. Restricted RHF-RCCSD(T) and RMP2 energies were

used for open-shell species; RHF-RCCSD(T) stands for partially spin-adapted open-shell coupled cluster singles and doubles theory augmented with a perturbation correction for triple excitations starting from molecular orbitals obtained from restricted open shell Hartree−Fock calculations. For coupled cluster calculations, the degree of a multireference character of wave functions was monitored through T1 diagnostics. The theoretical method used is normally capable to provide a chemical accuracy of 3–6 kJ mol^{-1} for the relative energies and 0.01–0.02 Å for bond lengths as well as 1–2° for bond angles.[38] The GAUSSIAN 09[39] and MOLPRO 2021[40] program packages were used for the B3LYP and G3(MP2,CC) calculations, respectively. – The Rice-Ramsperger-Kassel-Marcus (RRKM) theory,[38,41,42] was used for the calculations of energy-dependent rate constants of all unimolecular steps in the [4]helicenyl + C_4H_4 and [5]helicenyl + C_4H_4 following the formation of the initial intermediates **[i3]** and **[i12]**, respectively, at zero collision energy and in the limit of zero pressure corresponding to the conditions in cold molecular clouds. Note that under such conditions, only **[i3]** can be produced in the [4]helicenyl + C_4H_4 reaction where the vinylacetylene moiety adds to the radical site in the aromatic ring by its vinylic end. Alternatively, in the [5]helicenyl + C_4H_4 reaction, both additions by the vinylic and acetylenic ends feature submerged barriers and hence RRKM calculations began from the van-der-Waals complex **[i12]**. The computed rate constants were utilized to evaluate product branching ratios under cold molecular clouds conditions within steady-state approximation.[43]

Astrochemical Models. To study the chemistry of PAHs containing up to six six-membered rings in the cold molecular cloud TMC-1, we built the chemical model by expanding the RATE12 network [44] with barrierless neutral – neutral reactions leading to PAHs and their precursors. First, a fiducial time-dependent gas-phase model was operated [44] until the chemistry evolves to steady-state, i.e. after typically 10^7 years. The molecular abundances at this point are then employed as the initial conditions for the next step.

Second, the simulations were conducted over multiple runs with the ice mantle species injected into the gas phase through reactive desorption until it reaches the steady state; this strategy was exploited successfully to demonstrate the key role of neutral- neutral reactions in the formation of benzene in TMC-1.[45] These results were then benchmarked with astronomical observations for cyanobenzene (C_6H_5CN), and 1- and 2-cyanonapthalene ($C_{10}H_8CN$) to verify the predictive capabilities of the chemical network (†ESI).

Results & Discussion

Molecular Beams Experiments – Identification of the Molecular Formula of the Product. A chemical micro reactor was utilized to prepare [5]helicene via the gas phase reaction of the benzo[*c*]phenanthren-2-yl radical ($C_{18}H_{11}^{\bullet}$) with vinylacetylene (C_4H_4) (Figure 2a inset). The reaction products were probed isomer-specifically in a molecular beam via tunable vacuum ultraviolet (VUV) light followed by detection of the ionized molecules in a reflectron time-of-flight mass spectrometer (Re-TOF-MS) (Methods). An illustrative mass spectrum recorded at a photoionization energy of 9.50 eV for the reaction of the benzo[*c*]phenanthren-2-yl radical ($C_{18}H_{11}^{\bullet}$) with vinylacetylene (C_4H_4) is shown in Figure 2 b; reference data were also collected by replacing the vinylacetylene reactant with non-reactive helium carrier gas (Figure 2 a). A detailed comparison of these data reveals compelling evidence for the preparation of a molecule with the molecular formula $C_{22}H_{14}$ (278 amu) along with its ^{13}C counterpart $^{13}CC_{21}H_{14}$ (279 amu) in the benzo[*c*]phenanthren-2-yl – vinylacetylene system (Figure 2b, inset). Considering the molecular weight of the reactants and of the products, the $C_{22}H_{14}$ isomer(s) along with a light hydrogen atom represents the outcome of the reaction of the benzo[*c*]phenanthren-2-yl radical ($C_{18}H_{11}^{\bullet}$; 227 amu) with vinylacetylene (C_4H_4; 52 amu) (reaction (1)). Additional ion counts from m/z = 226 to 229 and 306–309 are observed in both the benzo[*c*]phenanthren-2-yl – vinylacetylene system *and* in the control experiment; this finding suggests that the

generation of these species does not require molecular mass growth processes through the reaction of the benzo[*c*]phenanthren-2-yl radical with vinylacetylene (†ESI; Figure S1).

Molecular Beams Experiments – Identification of the Structural Isomers of the Products. The nature of the structural isomer(s) at *m/z* of 278 ($C_{22}H_{14}^+$) prepared in the reaction of the benzo[*c*]phenanthren-2-yl radical with vinylacetylene is revealed by the detailed examination of the corresponding photoionization efficiency (PIE) curve, which portrays the intensity of the ion as a function of the photon energy from 7.00 eV to 9.50 eV (Figure 3a). The experimental PIE curve at *m*/*z* = 278 (Figure 3, black line) can only be fit with a linear combination of known reference PIE curves of distinct isomers of $C_{22}H_{14}$ such as [5]helicene (Figure 3, green line) and benzo[a]tetraphene (Figure 3, blue line). The experimental and reference PIE curves for [5]helicene reveal an onset of the ion signal at 7.40 ± 0.05 eV. However, the PIE curve of [5]helicene alone cannot replicate the ion counts beyond 8.50 eV. Considering the error bars, the contribution of benzo[*a*]tetraphene is clearly required to account for the lack of ion counts from the range of 7.00 eV to 8.50 eV. The overall fit (red) consists of ion counts of [5]helicene (82 ± 5 %) and of benzo[*a*]tetraphene (18 ± 4 %). It is important to note that the actual branching ratios of [5]helicene versus benzo[*a*]tetraphene require the knowledge of their photoionization cross sections; these are unknown. Electronic structure theory has not advanced to such a level to accurately compute the photoionization cross sections of organic molecules as complex as [5]helicene and benzo[*a*] tetraphene. Nevertheless, our experiments reveal the proof-of-concept that the reaction of benzo[*c*] phenanthren-2-yl radical with vinylacetylene leads to two distinct product isomers via molecular mass growth processes: benzo[*a*]tetraphene (**p1**) and [5]helicene (**p2**). It is critical to highlight that the PIE curve recorded at *m*/*z* = 279 (Figure 3b) can be associated with ^{13}C substituted isomer ($C_{17}{}^{13}CH_{12}$) of [5]helicene and benzo[*a*]tetraphene with an overall ion count intensities of 22 ± 2 % as predicted from the 1.1 % ^{13}C natural abundance along with 22 carbon atoms in the products.

Electronic Structure Calculations – [5]Helicene and its Isomers. With the experimental determination of distinct isomers [5]helicene and benzo[*a*]tetraphene ($C_{22}H_{14}$), we turn to electronic structure calculations to decipher the pathways that lead to their formation across complex potential energy surfaces. The computations were carried out at the G3(MP2,CC)//B3LYP/6–311G(d,p) level of theory and reveal that the [4]helicenyl radical may approach the vinylacetylene reactant barrierlessly resulting in the formation of two possible van-der-Waals complexes [**i1**] and [**i2**] (Figure 4; Table S1). These complexes are stabilized by 9 and 14 kJ mol^{-1} with respect to the separated reactants and reveal a carbon-carbon distance between the radical center of the benzo[*c*]phenanthren-2-yl radical with the vinyl (C1) and acetylenic (C4) carbon atoms of vinylacetylene of 409 and 388 pm, respectively. The van-der-Waals complexes can isomerize through addition of the radical center to the vinyl (C1) and acetylenic (C4) moieties via barriers of 3 and 16 kJ mol^{-1} yielding intermediates [**i3**] and [**i4**], respectively. A key feature of the addition to the C1 carbon atom is that the transition state to addition lies 6 kJ mol^{-1} *below* the energy of the separated reactants. Therefore, an addition barrier exists, but is lower in energy than the separated reactants and hence is termed a submerged barrier.[46] Whereas [**i3**] and [**i4**] may undergo unimolecular decomposition via atomic hydrogen loss to 2-((*E*)-but-1-en-3-ynyl)[4] helicene (**p3**) and 2-(but-3-en-1-ynyl)[4]helicene (**p4**), respectively, the resonantly stabilized doublet radical intermediate [**i3**] is fundamental in the formation of [5]helicene (**p2**) and benzo[*a*]tetraphene (**p1**). Benzo[*a*]tetraphene (**p1**) can be accessed via the reaction sequence [**i3**] → [**i5**] → [**i6**] → [**i7**] → **p1** + H, whereas [5]helicene (**p2**) can be prepared via [**i3**] → [**i8**] → [**i9**]/[**i10**] → [**i11**] → **p2** + H involving hydrogen atom shifts and a six-membered ring closure terminated by hydrogen atom losses from the methylene (CH_2) moieties in [**i7**] and [**i11**] through tight transition states located 19 and 20 kJ mol^{-1} above the energy of the separated products in overall exoergic reactions ($\Delta_R G$ (**p1**+H) = – 262 kJ mol^{-1}; $\Delta_R G$ (**p2**+H) = – 261 kJ mol^{-1}). A detailed analysis of the barriers of

isomerization of [**i3**] suggests that [5]helicene (**p2**) is formed preferentially. This deduction gains full support from the theoretically predicted branching ratios of 0.002 % : 99.8 % : 0.2 % for **p3** versus **p2** versus **p1** for cold molecular clouds conditions at 10 K and nearly zero pressure thus amplifying the synthetic route to [5]helicene (**p2**) in low temperature conditions of deep space (10 K). The presence of the submerged barrier is critical since these low temperatures effectively block reactions proceeding via transitions states located above the energy of the separated reactants such as the isomerization of **[i2]** to **[i4]** thus inhibiting the formation of 2-(but-3-en-1-ynyl)[4]helicene (**p4**). Recall that the thermodynamically less stable isomer **p3** was not detected in our study. Consequently, isomerization of [**i3**] and formation of [5]helicene (**p2**) and benzo[*a*]tetraphene (**p1**) is preferred at the expense of unimolecular decomposition to 2-((*E*)-but-1-en-3-ynyl)[4]helicene (**p3**). It is interesting to note that in case of a chiral [4]helicenyl reactant, its reaction with vinylacetylene should form a racemic mixture of [5]helicene. The memory of a particular chirality of the reactant is lost in the intermediate **[i8]**, which exhibits a planar geometry of the four aromatic rings due to the absence of an H atom at the most crowded position on one of the terminal rings. **[i8]** is still chiral due the presence of the CH_2CH_2CCH side chain but it can easily interconvert to its other enantiomer by facile rotation around the out-of-ring single C–CH_2 bond. Therefore, two different enantiomers of **[i11]** are predicted to be formed in nearly equal amounts and these enantiomers, after losing a hydrogen atom, would give rise to a racemic mixture of the product [5]helicene (**p2**). Alternatively, the particular chirality of the reactant is preserved along the entire reaction pathway toward **p1**; here, the chirality of benzo[*a*]tetraphene will coincide with that of the [4]helicenyl reactant.

Electronic Structure Calculations – [6]Helicene and its Isomers. The concept of a *de-facto* barrierless, vinylacetylene-mediated ring annulation to [4]helicenyl radicals leading to [5]helicene through resonantly stabilized free radical intermediates can be exported to

[6]helicene. This mechanism provides a unified and versatile synthetic route to racemic helicenes via successive molecular mass growth processes through bimolecular gas-phase reactions one ring at a time. The key features of the [5]helicenyl – vinylacetylene PES (Figure 5; Table S1) fundamentally mirror the [4]helicenyl – vinylacetylene system (Figure 4). The reaction is initiated through the formation of a van-der-Waals complex [**i12**]. Although two distinct long-range complexes could be located in the [4]-helicenyl-vinylacetylene system, despite an extensive search, only a single van-der-Waals complex was characterized in the reaction of [5]helicenyl with vinylacetylene with distances of at least 400 pm between the radical center and the vinyl and acetylene functional groups. This complex can isomerize through addition of the radical center of [5]helicenyl to the acetylenic or vinyl functional group forming [**i13**] or the resonantly stabilized free radical intermediate [**i14**], respectively. In both cases, the barriers to addition are located below the energy of the separated reactants; therefore, these can be once again be classified as submerged barriers. While [**i13**] may fragment via atomic hydrogen loss to 2-(but-3-en-1-ynyl)[5]helicene (**p5**), the chemistry of [**i14**] is more diverse. This intermediate either eliminates a hydrogen atom to form 2-((*E*)-but-1-en-3-ynyl)[5]helicene (**p6**) or undergoes hydrogen migration from the ortho or para position with respect to the side chain added to the benzene moiety yielding [**i15**] and [**i16**], respectively. These structures isomerize via ring closure to [**i17**] and [**i18**] followed by another hydrogen migration from the methylene group (CH_2) neighboring the carbene carbon atom to the latter; these shifts form intermediates [**i19**] and [**i20**], when then undergo hydrogen loss from the remaining methylene functional group accompanied by aromatization to [6]helicene (**p7**) and naphtho[1,2-a]tetraphene (**p8**) in overall exoergic reactions ($\Delta_R G$ (**p7**+H) = – 269 kJ mol^{-1}; $\Delta_R G$ (**p8**+H) = – 263 kJ mol^{-1}). The energies of the transition states for isomerization (or fragmentation) of [**i4**] along with the location of the barriers of the subsequent isomerization processes as discussed above advocate a favorable yield of [6]helicene (**p7**). Indeed, the computed branching ratios of 9.0 % : 0.04 % : 87.5 % : 3.4 % for **p5** versus **p6**

versus **p7** versus **p8** for cold molecular clouds (10 K) are in line with our hypothesis. The chirality of the [5]-helicenyl reactant is maintained along all reaction pathways and hence will be the same in particular for the [6]helicene (**p7**) and naphto[1,2-*a*]tetraphene (**p8**) products.

Astrochemical Modeling. Having provided compelling evidence on the formation of [5] and [6]helicene through *barrierless* reactions of the helicenyl radicals with vinylacetylene (reactions (1) and (2)), we are applying these findings now to 'real' cold molecular clouds. It is important to highlight that both reactions have no entrance barriers, all barriers involved in the isomerization processes are below the energy of the separates reactants, and the overall reactions (1) and (2) to [5] and [6]helicene are exoergic. These findings denote key requirements for both reactions to proceed in low-temperature environments such as in molecular clouds (10 K). Any barrier located above the energy of the separated reactants would inhibit the reactions to [5] and [6]helicene in molecular clouds; likewise, the low temperatures of the molecular clouds would prohibit endoergic reactions. In this context it is important to emphasize that although the reaction of the 4-phenanthrenyl radical ($C_{14}H_9^{\bullet}$) with vinylacetylene yields [4]helicene ($C_{18}H_{12}$),[28] the inherent barrier to addition in the entrance channel of 9 kJ mol^{-1} – equivalent to about 800 K – cannot be overcome in cold molecular clouds. This barrier is essentially the result of the sterical hindrance and hence repulsion between the first aromatic ring of the 4-phenanthrenyl radical and the vinylacetylene molecule adding with the methylidene moiety (CH_2) to the aryl radical center. In our present study, the sterical hindrance for the reactions of the [4] and [5]helicenyl radicals with vinylacetylene is significantly reduced due to the positioning of the attacked radical site outside of the molecular "bay" thus lowering the barrier heights below the energy of the separated reactants hence resulting in a submerged barrier. In this sense, the features in the entrance channels of the reactions to [5] and [6]helicene are quite distinct from those of the reaction of the 4-phenanthrenyl radical ($C_{14}H_9$) with

vinylacetylene (C_4H_4) leading to [4]helicene.[28] To explore the implications of our findings to the chemistry of aromatic hydrocarbons in cold molecular clouds, we explored the viability of the formation of polycyclic aromatic hydrocarbons via neutral-neutral reactions exploiting the University of Manchester Institute for Science and Technology (UMIST) Database (RATE2012).[44] The models were operated with physical parameters updated from References [44] and [47]: a cosmic ray ionization rate of 1.3×10^{-17} s^{-1}, a temperature of 10 K, a visual extinction of 10 Mag, and a number density of molecular hydrogen of 10^4 cm^{-3}. This network was updated with recently explored barrierless and rapid reactions related to the formation of benzene (C_6H_6),[45] naphthalene ($C_{10}H_8$),[46] phenanthrene ($C_{14}H_{10}$),[48] and [4]helicene[49] along with the channels to [5]helicene and [6]helicene elucidated in the present work (Figure 6, Table S2). Reaction pathways to benzene (C_6H_6) were extracted from Reference [45] (Materials and Methods; †ESI).

These modeling studies reveal fascinating conclusions. *First*, the performance of the astrochemical model for the cold molecular cloud TMC-1 can be benchmarked for the cyano derivatives of benzene (C_6H_6) and naphthalene ($C_{10}H_8$), i.e. cyanobenzene (C_6H_5CN), and 1- and 2-cyanonapthalene ($C_{10}H_8CN$), which were recently observed at fractional abundances of $4 \pm 1.6 \times 10^{-11}$ [50] as well as $7.35\,^{+3.33}_{-4.63} \times 10^{-11}$ and $7.05\,^{+3.23}_{-4.50} \times 10^{-11}$ toward TMC-1.[51] Formed predominantly via the barrierless reactions of benzene and naphthalene with cyano radicals,[52,53] the predicted peak fractional abundances at 2×10^5 years of cyanobenzene (C_6H_5CN) and both cyanonapthalene ($C_{10}H_8CN$) isomers with respect to molecular hydrogen reproduce the astronomical observations exceptionally well (Figure 7). *Second*, barrierless molecular mass growth processes via ring annulation lead from two-ring PAHs ($C_{10}H_8$; naphthalene) via three ($C_{14}H_{10}$; phenanthrene), four ($C_{18}H_{12}$; [4]helicene), five ($C_{22}H_{14}$; [5]helicene), and six-ring PAHs ($C_{26}H_{16}$; [6]helicene). With increasing complexity, the fractional abundances decrease from a few 10^{-8} for naphthalene via 2×10^{-9} for phenanthrene and 3×10^{-10} for [4]helicene to nearly 10^{-11} for [5]helicene

and 8×10^{-14} for [6]helicene. This implies that in future observations, at least three to five ringed PAHs including [4] and [5]helicenes might be detectable by radio telescopes.

Conclusion

Our combined experimental, computational, and astrochemical modeling results provided compelling evidence on a versatile, barrierless molecular mass growth process to helicenes via ring annulation in cold molecular clouds (10 K) as the result of bimolecular reactions of helicenyl radicals with vinylacetylene in the gas-phase. Commencing with the photolysis of an [*n*]helicene [$C_{14+4n}H_{10+2n}$] to an [n]helicenyl radical [$C_{14+4n}H_{9+2n}$] through the internal ultraviolet field (reaction (3)),[54] this universal mechanism effectively converts an [*n*]helicene into an [*n*+1]helicene [$C_{14+4(n+1)}H_{10+2(n+1)}$] (reaction (4)).

(3) $$C_{14+4n}H_{10+2n} + h\upsilon \rightarrow C_{14+4n}H_{9+2n} + H$$

(4) $$C_{14+4n}H_{9+2n} + C_4H_4 \rightarrow C_{14+4(n+1)}H_{10+2(n+1)} + H$$

The gas-phase synthesis of helicenes may have profound implications for the origin of the chiral asymmetry of life and contemporary biorelevant molecules such as right-handed sugars and left- handed amino acids. Although the gas-phase processes unraveled here form *racemates* of [5] and [6]helicenes, in deep space, ultraviolet circularly polarized light may preferentially photolyze the **M** or **P** enantiomer; this process could lead to an enrichment of one enantiomer over the other (enantiomeric excess), which can be propagated by the further growth. Since PAHs, to which helicene belongs, represent fundamental molecular building blocks of nanometer-sized interstellar grains,[55-60] a bottom-up formation of carbonaceous nanoparticles via PAHs leads to chiral carbonaceous nanostructures[26,27,56,57,61] and may translate the enantiomeric excess of the helicenes from the gas-phase to the nanoparticles eventually resulting into *chiral islands* or *chiral surfaces*. Although there is no detailed description to date of how carbonaceous nanoparticles might form in deep space, PAHs are likely key contributors. Consequently, the work disseminated here signifies a critical advancement toward a systematic understanding of the fundamental

chemical processes forming carbonaceous grains in the interstellar medium. At low temperatures of cold molecular clouds (10 K), these grains accrete nanometer thick icy layers of, e.g., water, carbon monoxide, carbon dioxide, formaldehyde, methanol, methane, and ammonia.[62] Interaction of interstellar ices with ionizing radiation such as galactic cosmic rays and the internal ultraviolet field[63] revealed the synthesis of complex organic molecules of astrobiological significance such as amino acids,[11-15] dipeptides,[64] and even sugars at 10 K.[16] In the presence of *chiral islands* and *chiral surfaces*, a grain-surface-mediated synthesis may lead to an enantiomeric excess within the newly formed molecules like sugars and amino acids. Therefore, these biorelevant molecules, which have been enantiomerically enriched through a chiral surface-mediated low temperature ice-surface chemistry in molecular clouds, could have been eventually delivered to the early Earth. This scenario gains strong support from the recent identification of D-enriched sugar alcohols and sugar acids like arabinonic acid[7] along with L-enriched non-terrestrial amino acids such as isovaline, α-methyl norvaline, α-methyl valine, and α-methyl norleucine in Murchison and Murray carbonaceous meteorites[8] thus bringing us closer to the understanding of the origin of homochirality.

Data Availability

The datasets generated during this study are available upon request.

Acknowledgements

This work was supported by the U.S. Department of Energy, Basic Energy Sciences DE-FG02-03ER15411 (experimental studies; R.I.K., L.Z.) and DE-FG02-04ER15570 (computational studies; A.M.M.) to the University of Hawaii and Florida International University, respectively. W.L. and M.A. are supported by the Director, Office of Science, Office of Basic Energy Sciences, of the U.S. Department of Energy under Contract No.

DE-AC02-05CH11231, through the Gas Phase Chemical Physics program of the Chemical Sciences Division. The ALS is supported under the same contract. The calculations were also supported by the Ministry of Science and Higher Education of the Russian Federation under Grant No. 075-15-2021-597. We also acknowledge the National Energy Research Scientific Computing Center (NERSC) of the Office of Science in the U.S. Department of Energy for providing HPC computing resources that have contributed to the research results reported within this paper. X.L. acknowledges support from the Xinjiang Tianchi project (2019).

Author Contributions

R.I.K. designed the experimental program and guided the astrochemical models; W.L. and L.Z. performed the experiments under the supervision of M.A.; M.M.E., V.N.A., and A.M.M. conducted the electronic structure and RRKM calculations; R.K.M. synthesized the precursors under supervision by F.R.F.; R.I.K. and M.A. wrote the manuscript. X.L. conducted the astrochemical modeling.

Competing Interests

The authors declare no competing interests.

References

1. J. C. Aponte, J. P. Dworkin and J. E. Elsila, *Geochim. Cosmochim. Acta*, 2014, **141**, 331-345.
2. S. Pizzarello and E. Shock, *Orig. Life Evol. Biosph.*, 2017, **47**, 249-260.
3. V. Prelog, *Science*, 1976, **193**, 17-24.
4. A. Brack, *Chem. Biodiversity*, 2007, **4**, 665-679.
5. R. I. Scorei, V. M. Cimpoiaşu and R. Popa, *Astrobiology*, 2007, **7**, 733-744.
6. D. P. Glavin, A. S. Burton, J. E. Elsila, J. C. Aponte and J. P. Dworkin, *Chem. Rev.*, 2020, **120**, 4660-4689.
7. G. Cooper and A. C. Rios, *PNAS*, 2016, **113**, E3322-E3331.
8. S. Pizzarello and J. R. Cronin, *Geochim. Cosmochim. Acta*, 2000, **64**, 329-338.
9. D. P. Glavin and J. P. Dworkin, *PNAS*, 2009, **106**, 5487-5492.
10. M. H. Engel and S. A. Macko, *Nature*, 1997, **389**, 265-268.

11. P. D. Holtom, C. J. Bennett, Y. Osamura, N. J. Mason and R. I. Kaiser, *ApJ*, 2005, **626**, 940-952.
12. Y. Oba, Y. Takano, N. Watanabe and A. Kouchi, *ApJ*, 2016, **827**, L18.
13. H. B. Throop, *Icarus*, 2011, **212**, 885-895.
14. M. Nuevo, G. Auger, D. Blanot and L. d'Hendecourt, *Orig. Life Evol. Biosph.*, 2008, **38**, 37-56.
15. M. P. Bernstein, J. P. Dworkin, S. A. Sandford, G. W. Cooper and L. J. Allamandola, *Nature*, 2002, **416**, 401-403.
16. C. Meinert, I. Myrgorodska, P. d. Marcellus, T. Buhse, L. Nahon, S. V. Hoffmann, L. L. S. d'Hendecourt and U. J. Meierhenrich, *Science*, 2016, **352**, 208-212.
17. A. Bergantini, M. J. Abplanalp, P. Pokhilko, A. I. Krylov, C. N. Shingledecker, E. Herbst and R. I. Kaiser, *ApJ*, 2018, **860**, 108.
18. J. Van House, A. Rich and P. W. Zitzewitz, *Origins of Life*, 1984, **14**, 413-420.
19. J. M. Dreiling and T. J. Gay, *Phys. Rev. Lett.*, 2014, **113**, 118103.
20. P. Modica, C. Meinert, P. de Marcellus, L. Nahon, U. J. Meierhenrich and L. L. S. d'Hendecourt, *ApJ*, 2014, **788**, 79.
21. J. J. Flores, W. A. Bonner and G. A. Massey, *J. Am. Chem. Soc.*, 1977, **99**, 3622-3625.
22. K. Soai, T. Kawasaki and A. Matsumoto, *Acc. Chem. Res.*, 2014, **47**, 3643-3654.
23. H. Sugahara, C. Meinert, L. Nahon, N. C. Jones, S. V. Hoffmann, K. Hamase, Y. Takano and U. J. Meierhenrich, *BBA Proteins and Proteomics*, 2018, **1866**, 743-758.
24. C. D. Stevenson and J. P. Davis, *ACS Earth Space Chem.*, 2020, **4**, 2358-2365.
25. C. D. Stevenson and J. P. Davis, *J. Phys. Chem. A*, 2019, **123**, 9587-9593.
26. Y. Nakakuki, T. Hirose and K. Matsuda, *J. Am. Chem. Soc.*, 2018, **140**, 15461-15469.
27. T. Mori, *Chem. Rev.*, 2021, **121**, 2373-2412.
28. L. Zhao, R. I. Kaiser, B. Xu, U. Ablikim, W. Lu, M. Ahmed, M. M. Evseev, E. K. Bashkirov, V. N. Azyazov, M. V. Zagidullin, A. N. Morozov, A. H. Howlader, S. F. Wnuk, A. M. Mebel, D. Joshi, G. Veber and F. R. Fischer, *Nat. Commun.*, 2019, **10**, 1510.
29. M. Rickhaus, M. Mayor and M. Juríček, *Chem. Soc. Rev.*, 2016, **45**, 1542-1556.
30. J. Bailey, *Orig. Life Evol. Biosph.*, 2001, **31**, 167-183.
31. T. Fukue, M. Tamura, R. Kandori, N. Kusakabe, J. H. Hough, J. Bailey, D. C. B. Whittet, P. W. Lucas, Y. Nakajima and J. Hashimoto, *Orig. Life Evol. Biosph.*, 2010, **40**, 335-346.
32. L. Zhao, R. I. Kaiser, B. Xu, U. Ablikim, M. Ahmed, D. Joshi, G. Veber, F. R. Fischer and A. M. Mebel, *Nat. Astron.*, 2018, **2**, 413-419.
33. L. Zhao, R. I. Kaiser, B. Xu, U. Ablikim, M. Ahmed, M. M. Evseev, E. K. Bashkirov, V. N. Azyazov and A. M. Mebel, *Nature Astronomy*, 2018, **2**, 973-979.
34. F. Qi, *Proc. Combust. Inst.*, 2013, **34**, 33-63.
35. L. A. Curtiss, K. Raghavachari, P. C. Redfern, V. Rassolov and J. A. Pople, *J. Chem. Phys.*, 1998, **109**, 7764-7776.
36. A. G. Baboul, L. A. Curtiss, P. C. Redfern and K. Raghavachari, *J. Chem. Phys.*, 1999, **110**, 7650-7657.

37. L. A. Curtiss, K. Raghavachari, P. C. Redfern, A. G. Baboul and J. A. Pople, *Chem. Phys. Lett.*, 1999, **314**, 101-107.
38. J. I. Steinfeld, J. S. Francisco and W. L. Hase, *Chemical Kinetics and Dynamics. Prentice Hall, Englewood Cliffs*, 1982.
39. M. J. Frisch, G. W. Trucks, H. B. Schlegel, G. E. Scuseria, M. A. Robb, J. R. Cheeseman, G. Scalmani, V. Barone, B. Mennucci, G. A. Petersson, H. Nakatsuji, M. Caricato, X. Li, H. P. Hratchian, A. F. Izmaylov, J. Bloino, G. Zheng, J. L. Sonnenberg, M. Hada, M. Ehara, K. Toyota, R. Fukuda, J. Hasegawa, M. Ishida, T. Nakajima, Y. Honda, O. Kitao, H. Nakai, T. Vreven, J. J. A. Montgomery, J. E. Peralta, F. Ogliaro, M. Bearpark, J. J. Heyd, E. Brothers, K. N. Kudin, V. N. Staroverov, T. Keith, R. Kobayashi, J. Normand, K. Raghavachari, A. Rendell, J. C. Burant, S. S. Iyengar, J. Tomasi, M. Cossi, N. Rega, J. M. Millam, M. Klene, J. E. Knox, J. B. Cross, V. Bakken, C. Adamo, J. Jaramillo, R. Gomperts, R. E. Stratmann, O. Yazyev, A. J. Austin, R. Cammi, C. Pomelli, J. W. Ochterski, R. L. Martin, K. Morokuma, V. G. Zakrzewski, G. A. Voth, P. Salvador, J. J. Dannenberg, S. Dapprich, A. D. Daniels, O. Farkas, J. B. Foresman, J. V. Ortiz, J. Cioslowski and D. J. Fox, *Gaussian 09, Revision A.1, Gaussian, Inc., Wallingford CT, 2009.*, 2009.
40. H. J. Werner, P. J. Knowles, G. Knizia, F. R. Manby, M. Schütz, P. Celani, W. Györffy, D. Kats, T. Korona, R. Lindh, A. Mitrushenkov, G. Rauhut, K. R. Shamasundar, T. B. Adler, R. D. Amos, S. J. Bennie, A. Bernhardsson, A. Berning, D. L. Cooper, M. J. O. Deegan, A. J. Dobbyn, F. Eckert, E. Goll, C. Hampel, A. Hesselmann, G. Hetzer, T. Hrenar, G. Jansen, C. Köppl, S. J. R. Lee, Y. Liu, A. W. Lloyd, Q. Ma, R. A. Mata, A. J. May, S. J. McNicholas, W. Meyer, T. F. M. III, M. E. Mura, A. Nicklass, D. P. O'Neill, P. Palmieri, D. Peng, T. Petrenko, K. Pflüger, R. Pitzer, M. Reiher, T. Shiozaki, H. Stoll, A. J. Stone, R. Tarroni, T. Thorsteinsson, M. Wang and M. Welborn, *MOLPRO, version 2021.2, A Package of Ab Initio Programs*, 2021.
41. P. J. Robinson and K. A. Holbrook, *Unimolecular Reactions. Wiley: New York*, 1972.
42. H. Eyring, S. H. Lin and S. M. Lin, *Basic Chemical Kinetics. John Wiley and Sons, Inc., New York*, 1980.
43. V. V. Kislov, T. L. Nguyen, A. M. Mebel, S. H. Lin and S. C. Smith, *J. Chem. Phys.*, 2004, **120**, 7008-7017.
44. D. McElroy, C. Walsh, A. J. Markwick, M. A. Cordiner, K. Smith and T. J. Millar, *A&A*, 2013, **550**, A36.
45. B. M. Jones, F. Zhang, R. I. Kaiser, A. Jamal, A. M. Mebel, M. A. Cordiner and S. B. Charnley, *PNAS*, 2011, **108**, 452-457.
46. D. S. N. Parker, F. Zhang, Y. S. Kim, R. I. Kaiser, A. Landera, V. V. Kislov, A. M. Mebel and A. G. G. M. Tielens, *PNAS*, 2012, **109**, 53-58.
47. A. J. Markwick, T. J. Millar and S. B. Charnley, *ApJ*, 2000, **535**, 256-265.
48. M. J. Abplanalp, R. Frigge and R. I. Kaiser, *Sci. Adv.*, 2019, **5**, eaaw5841.
49. L. Zhao, R. I. Kaiser, B. Xu, U. Ablikim, M. Ahmed, M. M. Evseev, E. K. Bashkirov, V. N. Azyazov and A. M. Mebel, *Angew. Chem. Int. Ed.*, 2020, **59**, 4051-4058.
50. B. A. McGuire, A. M. Burkhardt, S. Kalenskii, C. N. Shingledecker, A. J. Remijan, E. Herbst and M. C. McCarthy, *Science*, 2018, **359**, 202-205.

51. B. A. McGuire, R. A. Loomis, A. M. Burkhardt, K. L. K. Lee, C. N. Shingledecker, S. B. Charnley, I. R. Cooke, M. A. Cordiner, E. Herbst, S. Kalenskii, M. A. Siebert, E. R. Willis, C. Xue, A. J. Remijan and M. C. McCarthy, *Science*, 2021, **371**, 1265-1269.
52. N. Balucani, O. Asvany, A. H. H. Chang, S. H. Lin, Y. T. Lee, R. I. Kaiser, H. F. Bettinger, P. v. R. Schleyer and H. F. S. III, *J. Chem. Phys.*, 1999, **111**, 7457-7471.
53. R. I. Kaiser and N. Balucani, *Acc. Chem. Res.*, 2001, **34**, 699-706.
54. E. Peeters, C. Mackie, A. Candian and A. G. G. M. Tielens, *Accounts of chemical research*, 2021, **54**, 1921-1933.
55. J. O. Oña-Ruales, Y. Ruiz-Morales and F. Alvarez-Ramírez, *ACS Earth Space Chem.*, 2021, **5**, 381-390.
56. S. Liu, *J. Phys. Chem. Lett.*, 2020, **11**, 8690-8696.
57. X. Xiao, S. K. Pedersen, D. Aranda, J. Yang, R. A. Wiscons, M. Pittelkow, M. L. Steigerwald, F. Santoro, N. J. Schuster and C. Nuckolls, *J. Am. Chem. Soc.*, 2021, **143**, 983-991.
58. A. G. G. M. Tielens, *Reviews of modern physics*, 2013, **85**, 1021-1081.
59. A. G. G. M. Tielens and L. J. Alternandola, *Physics and Chemistry at Low Temperatures*, 2011, **Chapter 11**, 341-380.
60. L. Gavilan Marin, S. Bejaoui, M. Haggmark, N. Svadlenak, M. de Vries, E. Sciamma-O'Brien and F. Salama, *ApJ*, 2020, **889**, 101.
61. J. M. Fernández-García, P. J. Evans, S. Filippone, M. Á. Herranz and N. Martín, *Acc. Chem. Res.*, 2019, **52**, 1565-1574.
62. A. C. A. E. Boogert, P., *ASP Conference Series*, 2004, **309**, 547-572.
63. C. R. Arumainayagam, R. T. Garrod, M. C. Boyer, A. K. Hay, S. T. Bao, J. S. Campbell, J. Wang, C. M. Nowak, M. R. Arumainayagam and P. J. Hodge, *Chem. Soc. Rev.*, 2019, **48**, 2293-2314.
64. R. I. Kaiser, A. M. Stockton, Y. S. Kim, E. C. Jensen and R. A. Mathies, *ApJ*, 2013, **765**, 111.

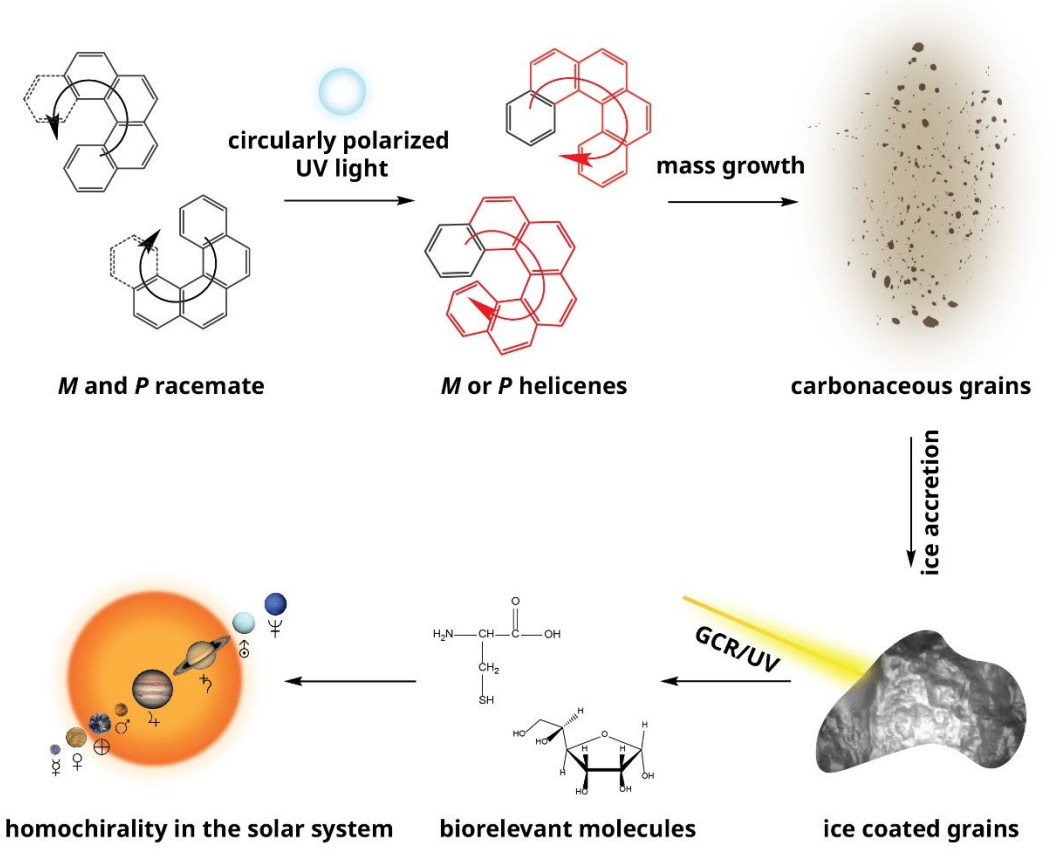

Fig 1. Overview of the role of racemic helicenes in the enantiomeric of sugars and amino acids in meteorites. Racemic mixtures of [5] and [6]helicenes can form in the gas-phase of the interstellar medium at ultralow temperatures in the absence of reaction barriers via molecular mass growth processes. Ultraviolet circularly polarized light may then preferentially photolyze one of the enantiomers leading to an enrichment of one enantiomer over the other. Polycyclic aromatic hydrocarbons (PAHs) – including enantiomerically enriched helicenes - can be incorporated into carbonaceous grains through molecular mass growth resulting into chiral islands or chiral surfaces. Upon interaction with galactic cosmic rays and ultraviolet photons, enantiomerically enriched complex organic molecules of astrobiological significance like sugars and aminoacids may be synthesized on ice coated chiral grains. Enantiomerically enriched biorelevant molecules could have been eventually delivered to early Earth. This brings us closer to the understanding of the origin of homochirality. GCR: Galactic Cosmic Rays; UV: Ultra Violet

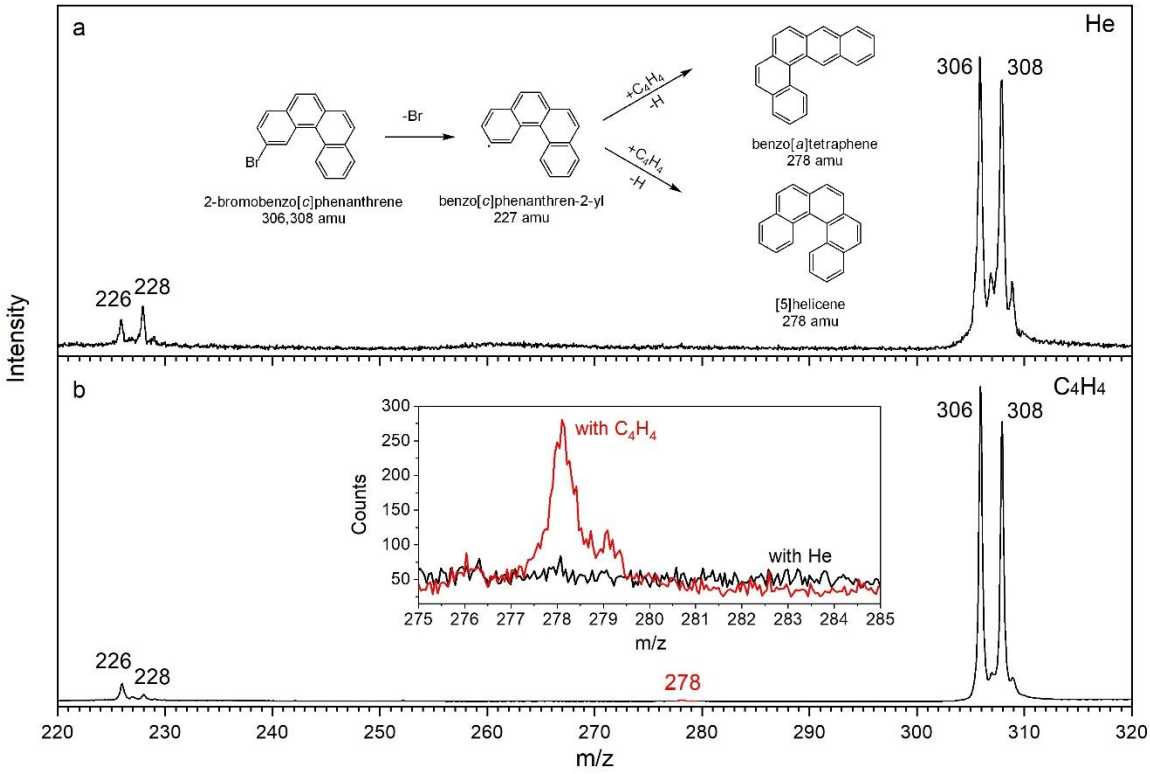

Fig 2. Comparison of photoionization mass spectra recorded at a photon energy of 9.50 eV. (a) 2-bromobenzo[*c*]phenanthrene ($C_{18}H_{11}Br$) - helium (He) system; (b) 2-bromobenzo[*c*] phenanthrene ($C_{18}H_{11}Br$) - vinylacetylene (C_4H_4) system. The inset of (a) represents the formation of benzo[*a*]tetraphene ($C_{22}H_{14}$) and [5]helicene ($C_{22}H_{14}$) from the reaction of the benzo[*c*]phenanthren-2-yl radical ($C_{18}H_{11}^{\bullet}$) with vinylacetylene (C_4H_4). The benzo[*c*]phenanthren-2-yl radical is produced from the pyrolysis of 2-bromobenzo[*c*]phenanthrene ($C_{18}H_{11}Br$). The inset of (b) shows the mass peak of the newly formed species of interest along with the ^{13}C-counterparts in red.

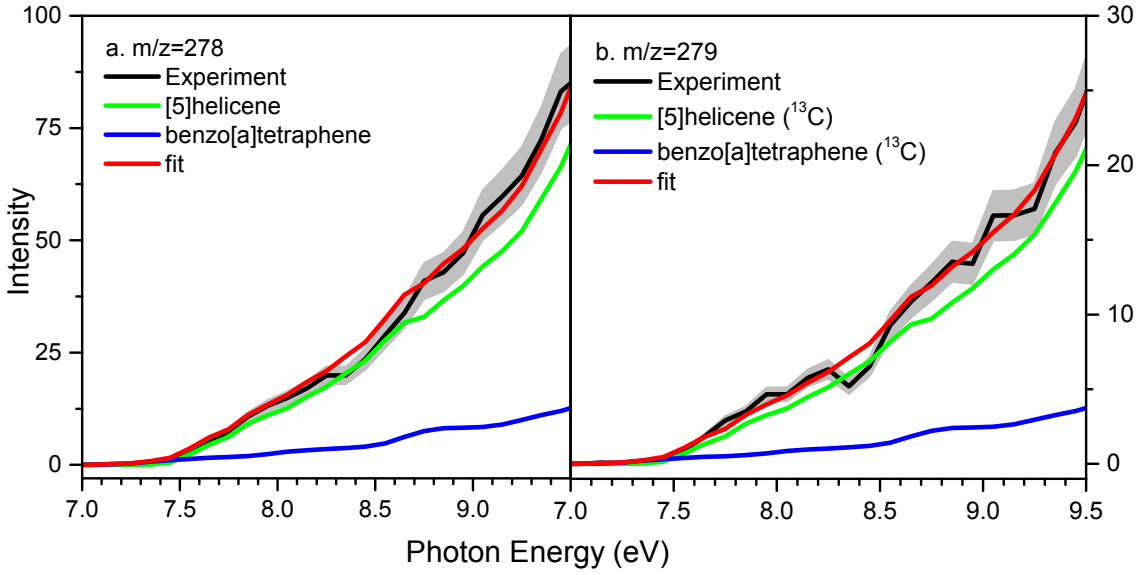

Fig 3. Photoionization efficiency (PIE) curves of *m*/*z* = 278 and 279 for the reaction of 2-bromobenzo[*c*]phenanthrene ($C_{18}H_{11}Br$) - vinylacetylene (C_4H_4). Black: experimentally derived PIE curves; colored lines (green and blue): reference PIE curves; red lines: overall fit. The overall error bars consist of two parts: ± 10 % based on the accuracy of the photodiode and a 1 σ error of the PIE curve averaged over the individual scans

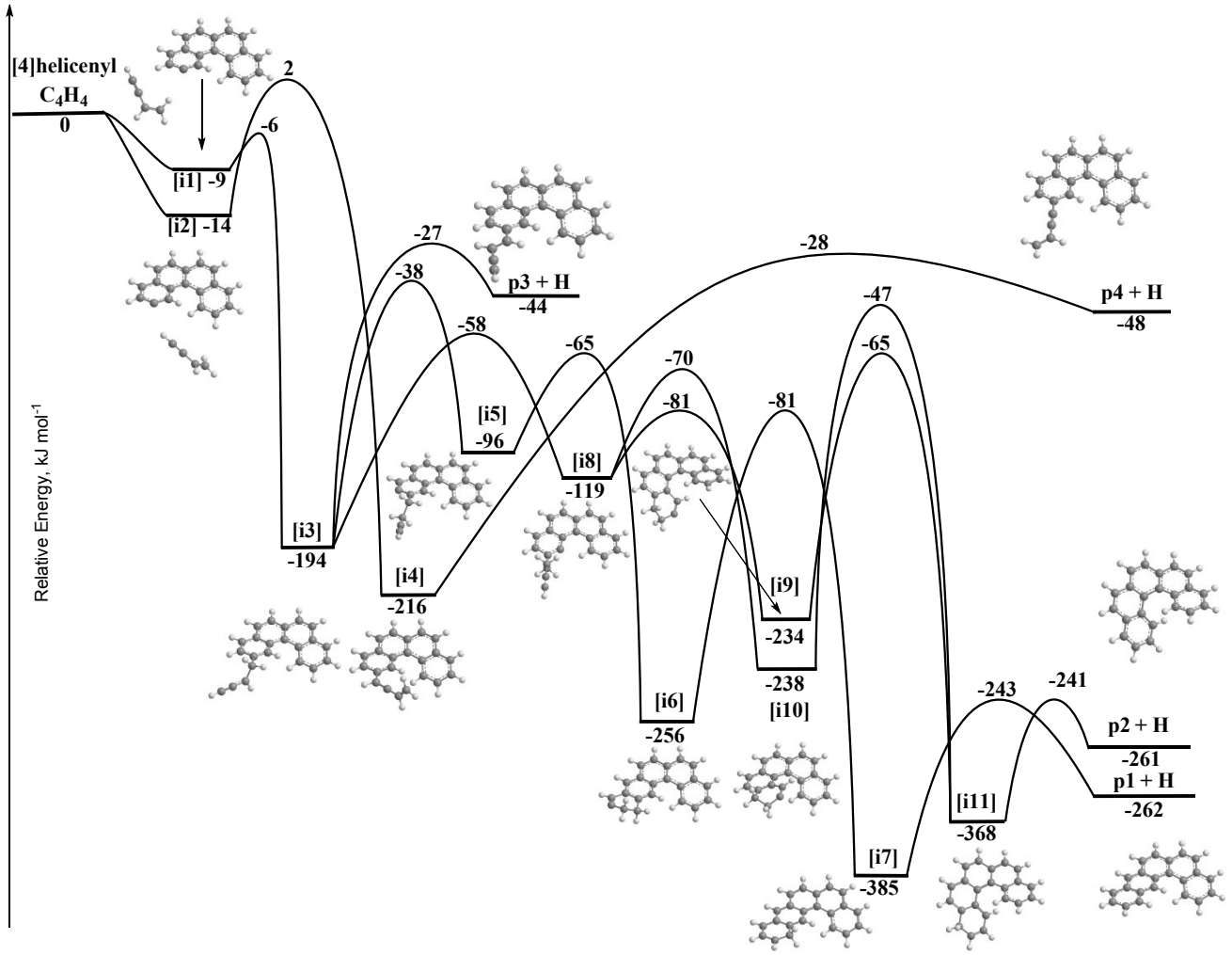

Fig 4. Potential energy surface (PES) for the [4]helicenyl ($C_{18}H_{11}$•) reaction with vinylacetylene (C_4H_4) leading to [5]helicene ($C_{22}H_{14}$). This PES was calculated at the G3(MP2,CC)//B3LYP/6-311G(d,p) level of theory. The relative energies are given in kJ mol^{-1}.

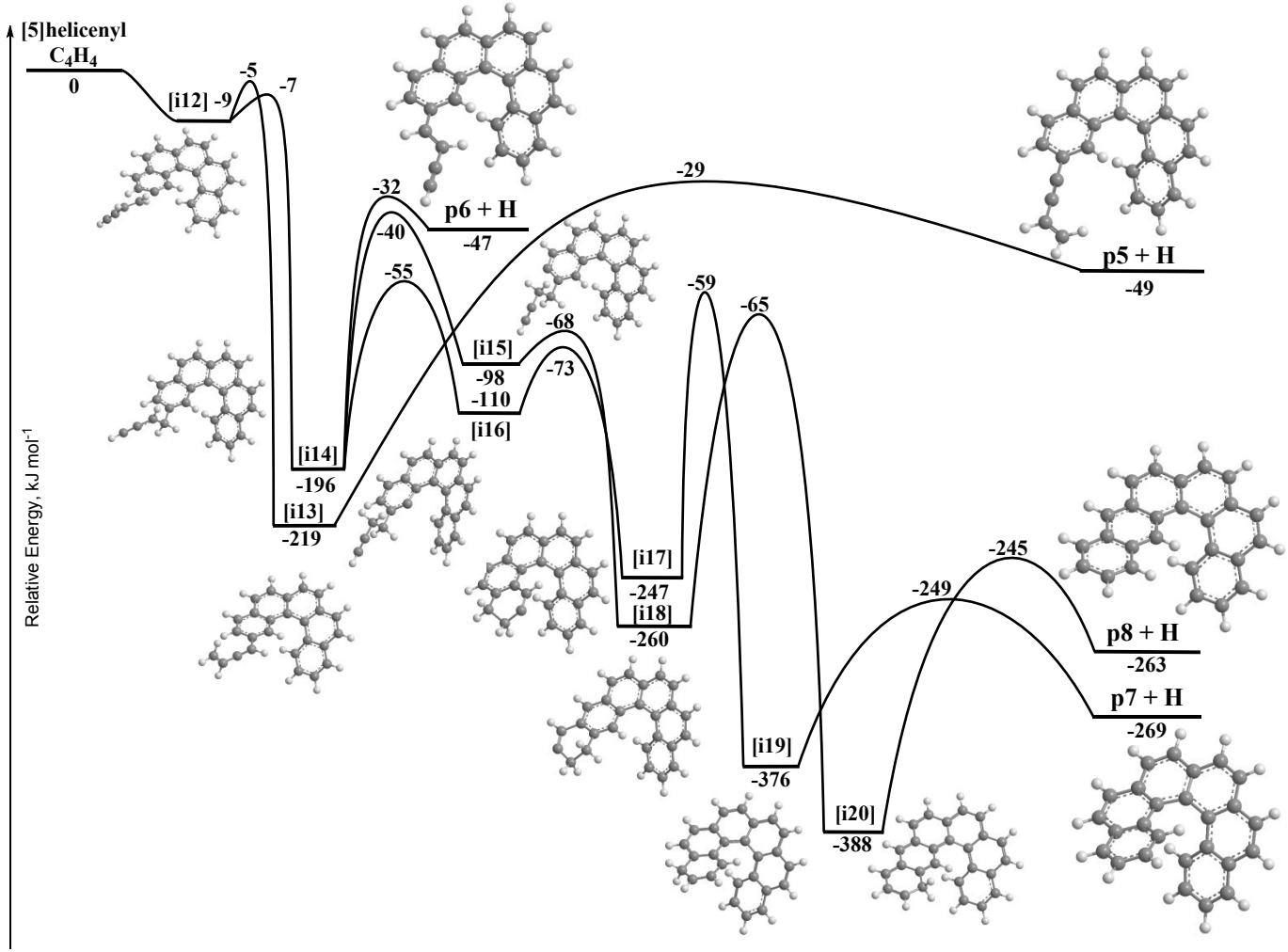

Fig 5. Potential energy surface (PES) for the [5]helicenyl ($C_{22}H_{13}$•) reaction with vinylacetylene (C_4H_4) leading to [6]helicene ($C_{26}H_{16}$). This PES was calculated at the G3(MP2,CC)//B3LYP/6-311G(d,p) level of theory. The relative energies are given in kJ mol^{-1}.

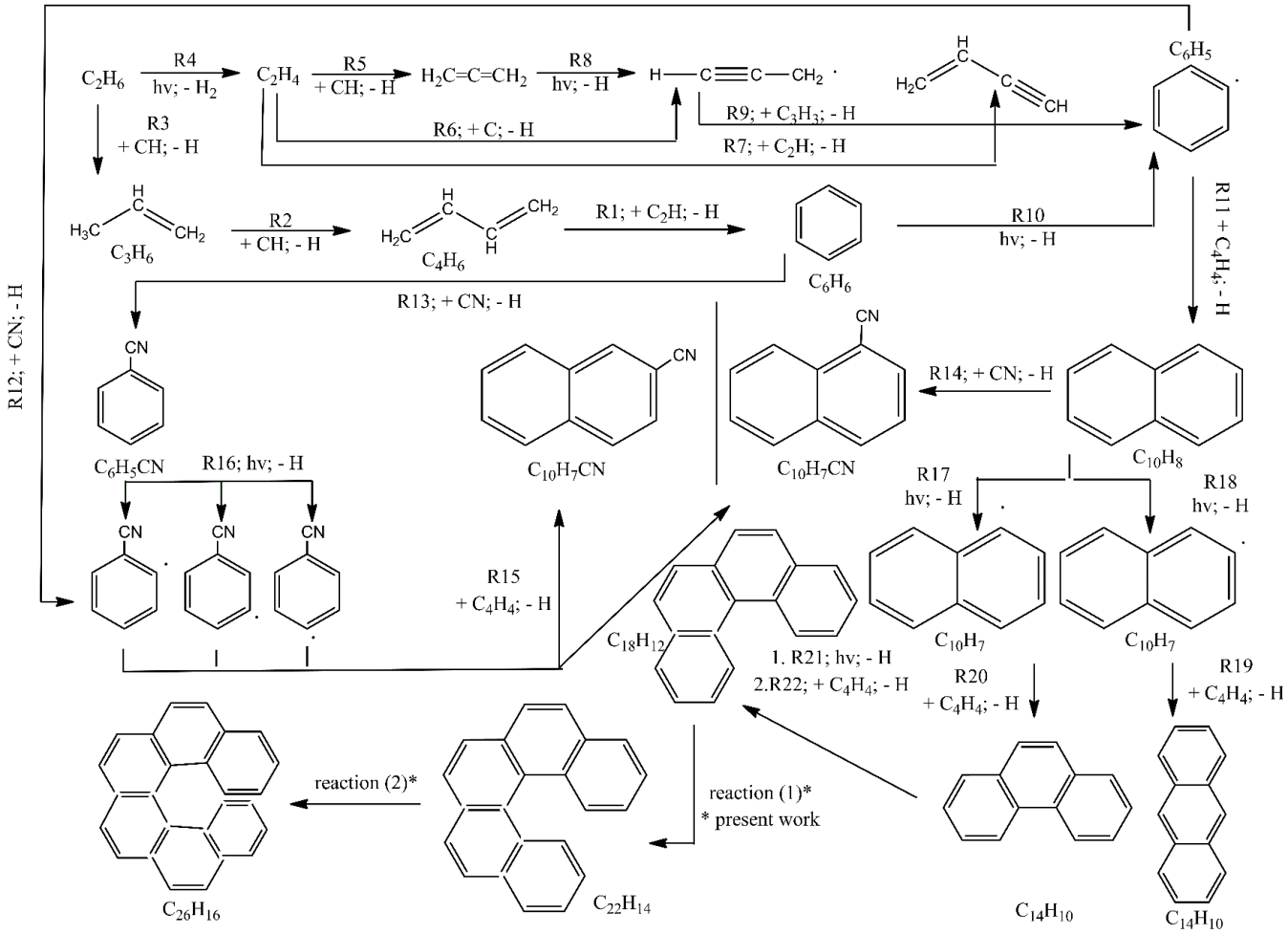

Fig. 6. Compilation of key bimolecular reactions leading to aromatic molecules as incorporated into the novel astrochemical models. The reactions R1-R22 are discussed in the Supplementary Information.

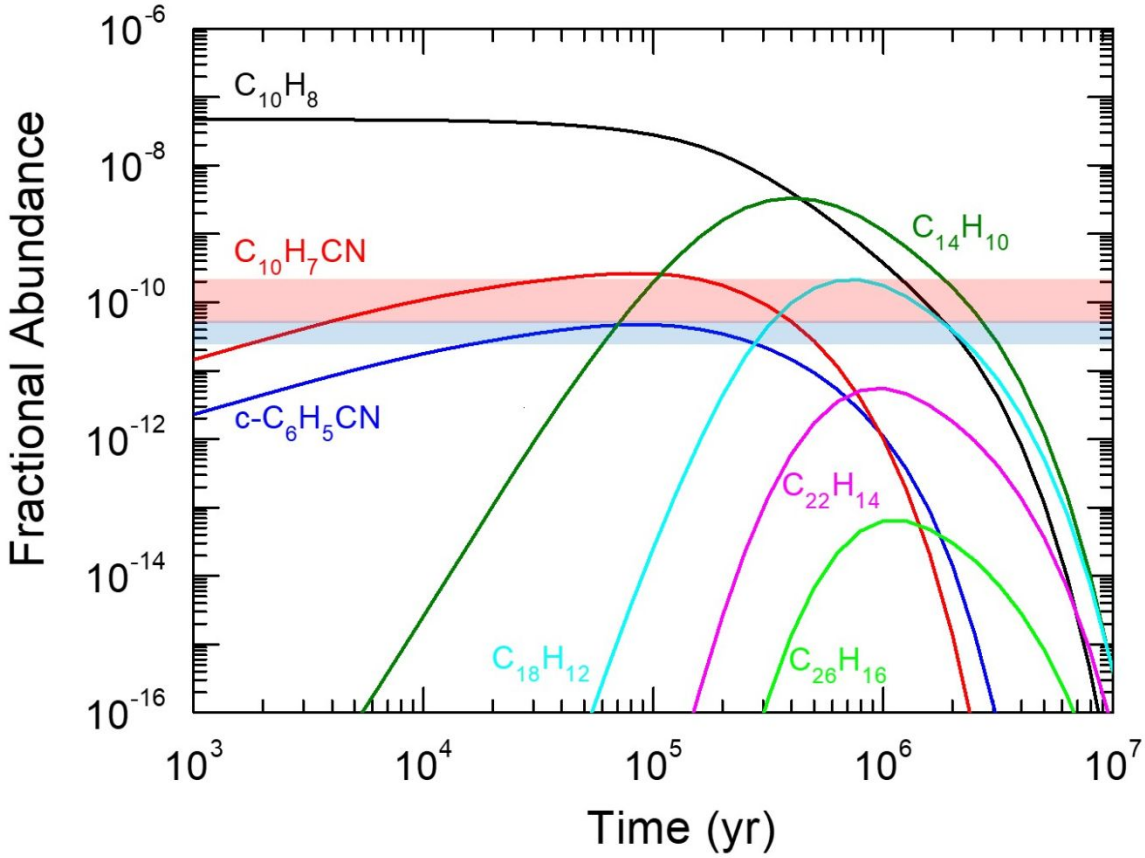

Fig. 7. Results of the astrochemical modeling for key pathways leading eventually to the formation of helicenes in TMC-1. The fractional abundances of the gas-phase species ($C_{10}H_8$; naphthalene), ($C_{14}H_{10}$; phenanthrene), ($C_{18}H_{12}$; [4]helicene), ($C_{22}H_{14}$; [5]helicene), and ($C_{26}H_{16}$; [6]helicene)) are plotted versus time for the cold molecular cloud TMC-1. Astronomically observed fractional abundances along with the uncertainties of cyanobenzene (C_6H_5CN) and cyanonapthalenes ($C_{10}H_7CN$) are visualized by the blue and red color-coded bars and agree nicely with the peak abundances predicted from the present models.